European Journal of Medicinal Chemistry 82 (2014) 355–362

Contents lists available at ScienceDirect

European Journal of Medicinal Chemistry

journal homepage: http://www.elsevier.com/locate/ejmech

Original article

Multifunctionalization of magnetic nanoparticles for controlled drug release: A general approach

Alfonso Latorre [1], Pierre Couleaud [1], Antonio Aires, Aitziber L. Cortajarena*, Álvaro Somoza*

Instituto Madrileño de Estudios Avanzados en Nanociencia & CNB-CSIC-IMDEA Nanociencia Associated Unit, Cantoblanco, Madrid, Spain

ARTICLE INFO

Article history:
Received 13 March 2014
Received in revised form
30 May 2014
Accepted 31 May 2014
Available online 2 June 2014

Keywords:
Magnetic nanoparticles
Multifunctionalization
Controlled drug release
Anticancer therapy
Disulfide bond
Nanomedicine

ABSTRACT

In this study, a general approach for the multifunctionalization of magnetic nanoparticles (MNPs) with drugs (Doxorubicin and Gemcitabine) and targeting moieties (Nucant pseudopeptide) for controlled and selective release is described. The functionalization is achieved by the formation of disulfide bonds between MNPs and drugs derivatives synthesized in this work. Our strategy consists in the introduction of a pyridyldisulfide moiety to the drugs that react efficiently with sulfhydryl groups of pre-activated MNPs. This approach also allows the quantification of the covalently immobilized drug by measuring the amount of the 2-pyridinethione released during the process. The linkers developed here allow the release of drugs without any chemical modification. This process is triggered under highly reducing environment, such as that present inside the cells.

Complete release of drugs is achieved within 5–8 h under intracellular conditions whereas negligible percentage of release is observed in extracellular conditions.

We propose here a modular general approach for the functionalization of nanoparticles that can be used for different types of drugs and targeting agents.

1. Introduction

The use of nanoparticles as carrier systems for therapeutic molecules has been explored during the last 20 years [1] aiming to improve the therapeutic effect of the drugs and their administration, as well as, to reduce their side effects. Different types of nanostructures (metallic nanoparticles, polymeric core–shell nanoparticles or micelles) have been evaluated particularly in cancer therapy, whose vast side effects compromise the health of patients. In this regard, nanoparticles can be designed as multifunctional platforms that can be loaded with several drugs and also modified with targeting molecules to direct them to cancer cells [2]. Targeted therapies have been developed to diminish side effects of current approaches [3] where specific cell membrane receptors overexpressed by cancer cells are used as targets, improving the efficacy of classical treatments [4,5].

Nanoparticles for medical applications, and particularly for targeted cancer therapy, must be (1) non-toxic (2) with a good colloidal stability in physiological conditions; (3) easy to load with known amounts of therapeutic agents and targeting molecules and (4) able to release the cargo efficiently inside the cells. Therefore, the development of strategies for the functionalization of nanoparticles is a crucial point for the future clinical use to improve anticancer therapies.

In this study, immobilization strategies for the functionalization of magnetic nanoparticles (MNP) using tailored linkers have been developed. The systems described have the required properties to be successfully employed in biomedical applications.

In particular, dimercaptosuccinic acid coated magnetic nanoparticles [6,7] (DMSA-MNPs) have been functionalized with two chemotherapeutic drugs and a targeting molecule. The controlled release of the drugs has been evaluated. One of the drugs employed is Doxorubicin (DOX), which is widely used to treat a broad spectrum of cancers (breast, stomach, non-Hodgkin's lymphoma, and bladder cancer) [8]. One advantage of DOX is its strong visible absorption and fluorescence emission that makes it easy to monitor during the different steps of the functionalization strategy. The other chemotherapeutic drug used is Gemcitabine (GEM) that is employed in several cancers such as pancreatic cancer [9–11], non-small cell lung cancer, bladder cancer, soft-tissue sarcoma, metastatic breast cancer and ovarian cancer and acts as an antineoplastic

* Corresponding authors.
E-mail addresses: aitziber.lopezcortajarena@imdea.org (A.L. Cortajarena), alvaro.somoza@imdea.org (Á. Somoza).
[1] Contributed equally to this work.

http://dx.doi.org/10.1016/j.ejmech.2014.05.078
0223-5234/

agent. Both drugs are cell-cycle specific therapeutic agents and therefore need to reach the nucleus. DOX acts by intercalating DNA whereas GEM replaces cytidine during DNA replication. Despite positive results with these drugs in clinics, classical chemotherapy still presents several problems. For example, doxorubicin has shown great efficacy in both solid and liquid tumors, but the emergence of drug resistance and several side effects such as heart muscle damage are important limitations for successful cancer treatment [12]. Gemcitabine undergoes rapid deamination into the inactive uracil derivative, resulting in a short half-life. Also in the case of Gemcitabine, drug resistance has been observed in *in vitro* and *in vivo* preclinical models, which is critical for future clinical usage [13]. The use of nanoparticle-based delivery systems has been shown to overcome multidrug resistance in tumors and to increase the stability immobilized molecules [14,15]. Therefore, more efficient nanoparticle-based formulations that additionally incorporate targeting for local administration are needed. In this sense, to introduce targeting capabilities in the multifunctional formulations the pseudopeptide Nucant (N6L) has been used together with DOX and GEM. The Nucant pseudopeptide, which acts both as an anticancer drug and as a targeting agent is nowadays in clinical trials. N6L binds nucleolin, which is a protein overexpressed in the membrane of cancer cells, and nucleophosmin [16,17], and can enter the cell nucleus to induce apoptosis [18].

As a first approach to improve cancer therapy non-covalent functionalization of nanoparticles, mainly through electrostatic or hydrophobic interactions [19,20] has been explored intensively in the past due to the ease of application, but has some concerns and drawbacks. The most important limitation is the poor control on the release of the drug immobilized onto such nanostructures. The drug release occurs as a passive process based on the high concentration of salts and biomolecules *in vivo* or on pH changes. This strategy is suitable for *in vitro* assays or *in vivo* assays using intratumoral injection but it should not be applied intravenously. Another drawback is the fact that neutral drugs under physiological conditions, such as Gemcitabine cannot be immobilized electrostatically.

Taking into account all these parameters, the covalent functionalization of anticancer drugs onto targeted nanoparticles seems to be a suitable way to tackle these problems. Ideally, only cancer cells should be targeted by drug-loaded magnetic nanoparticles, where anti-tumoral agents are inactivated until they are released inside the cell. In this regard, different linkers sensitive to certain intracellular triggering stimulus such as pH [21,22] and the presence of some enzymes [23–25], or external stimuli such as temperature [26,27] have been employed to connect and release drugs from magnetic nanoparticles in a controlled manner. On the other hand, disulfide bond based linkers have excellent properties for this application [28] because allow the formation of a covalent bond between the nanoparticle and the required molecule. Then, the disulfide bond can be broken by specific reducing agent such as endogenous glutathione (GSH). It is well known that the intracellular level of GSH in cells is in the millimolar range (0.5–10 mM), whereas just micromolar concentrations are typically found in blood plasma and the extracellular medium [29]. Moreover, it has been shown by clinical studies that tumor tissue is often higher in glutathione content than normal tissue [30,31]. By designing the functionalization with a disulfide linker, the attached molecule will be released only under highly reducing environment such as the tumor cells' intracellular environment. Another advantage of the strategy described here relies on the design of a modification attached to the molecules in order to quantify the immobilization. By anchoring a linker ending with a thiol activated by 2-mercaptopyridyl group, it is possible to quantify the amount of molecules linked to the nanoparticles by following the UV–Visible absorption of the byproduct released during the functionalization reaction. Finally, the linkers have been designed in order to release the molecule without any chemical modification, after an internal rearrangement [32,33]. Therefore, the initial molecule will be released within the cell and its activity will not be affected.

The work presented here is a successful example of efficient drug's covalent functionalization of nanoparticles for an intracellular controlled release. The method herein presented could be applied to other drugs (charged or neutral, fluorescent or not) and targeting agents (peptide, antibodies, etc.) for multiple biomedical applications.

2. Experimental

2.1. Materials

All reagents were purchased from Aldrich and used without further purification. José Courty's group from CRRET-CNRS laboratory provided cysteine modified Nucant pseudopeptide (N6L-Cys). Ultrapure reagent grade water (18.2 MΩ, Wasserlab) was used in all experiments. DMSA-MNPs have been provided by Dr. Gorka Salas' group at IMDEA Nanociencia.

2.2. Measurements

Thin layer chromatography (TLC) was carried out using Silica Gel 60 F254 plates. Column chromatography was performed using Silica Gel (60 Å, 230 × 400 mesh). All NMR spectra were recorded on a Bruker instrument (MHz indicated in brackets) as solutions in $CDCl_3$, and the chemical shifts are reported in parts per million (ppm). Coupling constants are reported in hertz (Hz). MALDI-TOF mass spectrometer analysis was performed using a Voyager DE Pro (AB Applied Biosystems). *UV–Vis* and fluorescence spectra were recorded on a Synergy H4 microplate reader (BioTek) using 96-well plates. Hydrodynamic diameter and zeta potential measurements were determined using a Zetasizer Nano-ZS device (Malvern Instruments). Hydrodynamic diameter and zeta potential were measured from dilute sample suspensions in water at pH 7.4 using a zeta potential cell. HPLC: Agilent Technologies, 1260 Infinity. Column ZORBAX 300SB-C18, 5 μm, 9.4 × 250 mm.

2.3. Synthesis and characterization

2.3.1. Synthesis of intermediates and drugs derivatives

2.3.1.1. Synthesis of 2-(pyridin-2-yldisulfanyl)ethanol (1) [32]. To a solution of aldrithiol (300 mg, 1.36 mmol) in MeOH (1.5 mL) under Ar, 2-mercaptoethanol (53 μL, 0.75 mmol) was added slowly and stirred for 16 h. Then, the solvent was evaporated in vacuum and the residue purified by flash chromatography (CH_2Cl_2/AcOEt 5:1) to obtain compound **1** (Fig. 1) as a colorless oil in 86% yield; ^{1}H NMR (300 MHz, $CDCl_3$) δ 8.51 (d, J = 4.3 Hz, 1H), 7.58 (td, J = 8.0, 1.7 Hz, 1H), 7.40 (d, J = 8.0 Hz, 1H), 7.17–7.13 (m, 1H), 5.72 (bs, 1H), 3.80 (dd, J = 10.4, 6.5 Hz, 2H), 2.97–2.94 (m, 2H).

2.3.1.2. Synthesis of 4-nitrophenyl 2-(pyridin-2-yldisulfanyl)ethyl carbonate (2) [32]. To a solution of compound **1** (100 mg, 0.53 mmol), and bis(4-nitrophenyl) carbonate (241 mg, 0.79 mmol) in CH_2Cl_2 (2 mL) under Ar, DIPEA (158 μL, 0.79 mmol) was added and stirred for 5 h. The mixture was washed with water, and the organic phase dried with $MgSO_4$. After solvent evaporation, the residue was purified by flash chromatography (Hexane/AcOEt 4:1 and then 2:1) to obtain compound **2** (Fig. 1) as a colorless oil 67% yield; ^{1}H NMR (300 MHz, $CDCl_3$) δ 8.50 (d, J = 4.8 Hz, 1H), 8.28 (d,

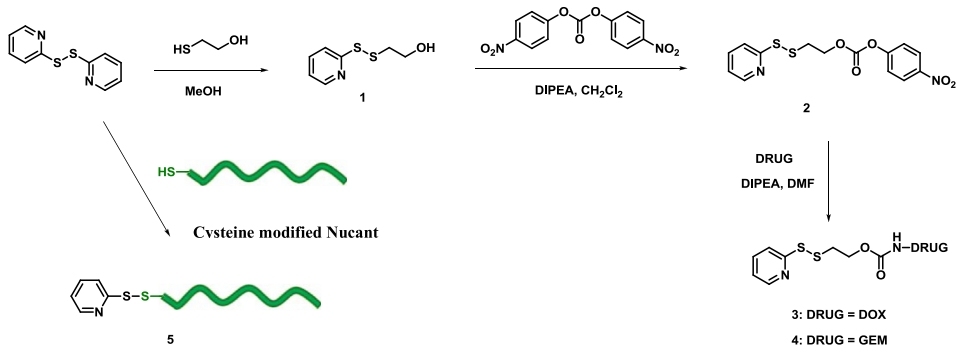

Fig. 1. General scheme of synthesis of drugs derivatives.

$J = 9.1$ Hz, 2H), 7.72–7.59 (m, 2H), 7.38 (d, $J = 9.1$ Hz, 2H), 7.15–7.10 (m, 1H), 4.57 (t, $J = 6.4$ Hz, 2H), 3.16 (t, $J = 6.4$ Hz, 2H).

2.3.1.3. Synthesis of doxorubicin derivative, DOX-S-S-Pyr (3) [33]. To a solution of compound **2** (10 mg, 0.028 mmol) and doxorubicin hydrochloride (12 mg, 0.020 mmol) in DMF (1 mL) under N_2, DIPEA (8 μL, 0.028 mmol) was added at room temperature and stirred for 16 h. Then, the solvent was evaporated and the residue was purified by flash chromatography (eluent: CH_2Cl_2/MeOH 20:1) to obtain compound **3** (Fig. 1) as red solid in 90% yield; ^{1}H NMR (500 MHz, $CDCl_3$) δ 13.94 (s, 1H), 13.18 (s, 1H), 8.40 (d, $J = 3.8$ Hz, 1H), 8.00 (d, $J = 7.6$ Hz, 1H), 7.76 (t, $J = 8.0$ Hz, 1H), 7.70 (d, $J = 7.5$ Hz, 1H), 7.63 (t, $J = 7.4$ Hz, 1H), 7.37 (d, $J = 8.5$ Hz, 1H), 7.07 (t, $J = 1$H), 5.50 b (s, 1H), 5.26 (dd, $J = 3.7$, 2.0 Hz, 1H), 5.15 (d, $J = 8.8$ Hz, 1H), 4.74 b (s, $J = 21.4$ Hz, 2H), 4.56 (bs, 1H), 4.42–4.34 (m, 1H), 4.21–4.08 (m, 2H), 4.06 (s, 3H), 3.81 (m, 1H), 3.62 (bs, 1H), 3.22 (dd, $J = 18.8$, 1.5 Hz, 1H), 3.14–2.86 (m, 5H), 2.33 (d, $J = 14.6$ Hz, 1H), 2.15 (dd, $J = 15.0$, 3.6 Hz, 1H), 1.81 (m, 2H), 1.48–1.42 (m, 2H), 1.29 (d, $J = 6.5$ Hz, 3H); ^{13}C NMR (126 MHz, $CDCl_3$) δ 213.9, 187.0, 186.6, 161.0, 160.1, 156.2, 155.6, 155.2, 149.8, 149.4, 137.3, 135.7, 135.4, 133.6, 133.6, 120.9, 120.8, 119.9, 119.8, 118.4, 111.5, 111.4, 100.9, 69.7, 69.0, 67.4, 65.6, 63.5, 56.7, 53.4, 47.0, 37.5, 35.6, 33.9, 30.0, 29.7, 28.3, 17.0; MS (ESI): *m/z* (%)757 (100).

2.3.1.4. Synthesis of Gemcitabine derivative, GEM-S-S-Pyr (4). To a solution of compound **2** (25 mg, 0.071 mmol) and Gemcitabine chlorhydrate (24 mg, 0.09 mmol) in DMF (1.5 mL) under Ar, DIPEA (18 μL, 0.09 mmol) and DMAP (catalytic amount) were added and stirred for 16 h. Then, the solvent was evaporated in vacuum and the residue purified by flash chromatography (CH_2Cl_2/MeOH 15:1) to obtain compound **4** (Fig. 1) in 38% yield as a colorless oil; ^{1}H NMR (500 MHz, $CDCl_3$) δ 8.44–8.43 (m, 1H), 7.70–7.64 (m, 2H), 7.52 (d, $J = 6.8$ Hz, 1H), 7.11 (ddd, $J = 6.7$, 4.9, 1.5 Hz, 1H), 6.23 (bs, 2H), 5.80 (d, $J = 7.5$ Hz, 1H), 5.33 (bs, 1H), 4.50–4.38 (m, 3H), 4.13 (d, $J = 7.5$ Hz, 1H), 4.04 (d, $J = 12.0$ Hz, 1H), 3.84 (d, $J = 12.0$ Hz, 1H), 3.13–3.02 (m, 2H); ^{13}C NMR (126 MHz, $CDCl_3$) δ 165.8, 159.2, 155.6, 153.5, 149.8, 149.6, 137.4, 121.1, 120.0, 95.7, 78.7, 78.7, 72.7, 66.8, 65.4, 59.6, 36.5; MS (ESI): *m/z* (%)239 (23), 477 (M^++H, 100), 499 (M^++Na, 2); HRMS (ESI) calculated for $C_{17}H_{19}F_2N_4O_6S_2$ (M^++H) 477.0708, found 477.0708; HRMS (ESI) calculated for $C_{17}H_{18}N_4O_6F_2NaS_2$ (M^++Na) 499.0547, found 499.0528.

2.3.1.5. Synthesis of Nucant-S-S-Pyr (5). To 1.2 mL of Nucant-Cys (600 μM) 400 μL of 2,2′-dipyridyldisulfide (30 mM in DMSO) were added and incubated during 4 h at room temperature (RT). The progress of the reaction was followed measuring the formation of 2-pyridinethione by UV absorption at 343 nm ($\varepsilon_{343\ nm}$ = 8080 L mol^{-1} cm^{-1}).

After the reaction was finished, a NAP-10 column was used to separate **5** from the excess of 2,2′-dipyridyldisulfide and DMSO. Nucant-S-S-Pyr (5) was collected in the first fractions, obtained with a yield of 70% and stored at −20 °C. Quantification of activated thiol moieties of the Nucant-S-S-Pyr was achieved by adding DDT on an aliquot and measuring the band at 343 nm due to 2-pyridinthione released (ε_{343nm} = 8080 L mol^{-1} cm^{-1}). MS (ESI): *m/z* (%), (M^+) found 4237.56 (100), calculated for $C_{190}H_{354}N_{71}O_{34}S_2$ (M^+) 4238.8.

2.3.2. Covalent attachment of drug derivatives to thiolated DMSA-MNPs

2.3.2.1. Pre-activation of DMSA-MNPs. DMSA-MNPs were first modified with cysteamine hydrochloride to introduce thiol moieties (thiolated DMSA-MNPs). To 1 mL of DMSA-MNPs at 2.4 mg Fe/mL were added 50 μmol of cysteamine hydrochloride/g Fe, previously neutralized by 1 equivalent of NaOH, 150 μmol of EDC/g Fe and 75 μmol of NHS/g Fe. After 16 h, the sample was washed by cycles of centrifugation and redispersion in milliQ water at least 3 times.

Thiolated DMSA-MNPs were used for the functionalization with the different molecules (DOX, GEM and N6L).

2.3.2.2. Reaction between thiolated DMSA-MNPs and Doxorubicin derivative (3). 1 mL of aqueous suspension of thiolated DMSA-MNPs at 2.4 mg Fe/mL was mixed with 240 μL of DOX-S-S-Pyr **(3)** solution at 500 μM in DMF (0.012 μmol) during 16 h at 37 °C. After this time, 20 μL of brine were added and the sample centrifuged 10 min at *5000* × *g*. From the collected supernatants, the covalently immobilized DOX onto thiolated DMSA-MNPs was determined by quantification of the 2-pyridinethione released (λ_{max} = 343 nm, $\varepsilon_{343\ nm}$ = 8080 L mol^{-1} cm^{-1}, Fig. S.1). Finally the sample was redispersed in 1 mL of MilliQ water.

2.3.2.3. Reaction between thiolated DMSA-MNPs and Gemcitabine derivative (4). 1 mL of aqueous suspension of thiolated DMSA-MNPs at 2.4 mg Fe/mL was mixed with 240 μL of GEM-S-S-Pyr **(4)** solution at 500 μM in DMF (0.012 μmol) during 16 h at 37 °C. After reaction, 20 μL of brine were added and the sample centrifuged 10 min at *5000* × *g*. From the collected supernatants, the covalently immobilized GEM onto thiolated DMSA-MNPs was determined by quantification of the 2-pyridinethione released (λ_{max} = 343 nm, $\varepsilon_{343\ nm}$ = 8080 L mol^{-1} cm^{-1}, Fig. S.2). Finally, the sample was redispersed in 1 mL of MilliQ water.

2.3.2.4. Synthesis of MNP-N6L conjugate. 1 mL of aqueous suspension of thiolated DMSA-MNPs at 2.4 mg Fe/mL was mixed with 84 μL of Nucant-S-S-Pyr **(5)** at 200 μM in water (0,0168 μmol) during 16 h at RT. The reaction mixture was centrifuged and

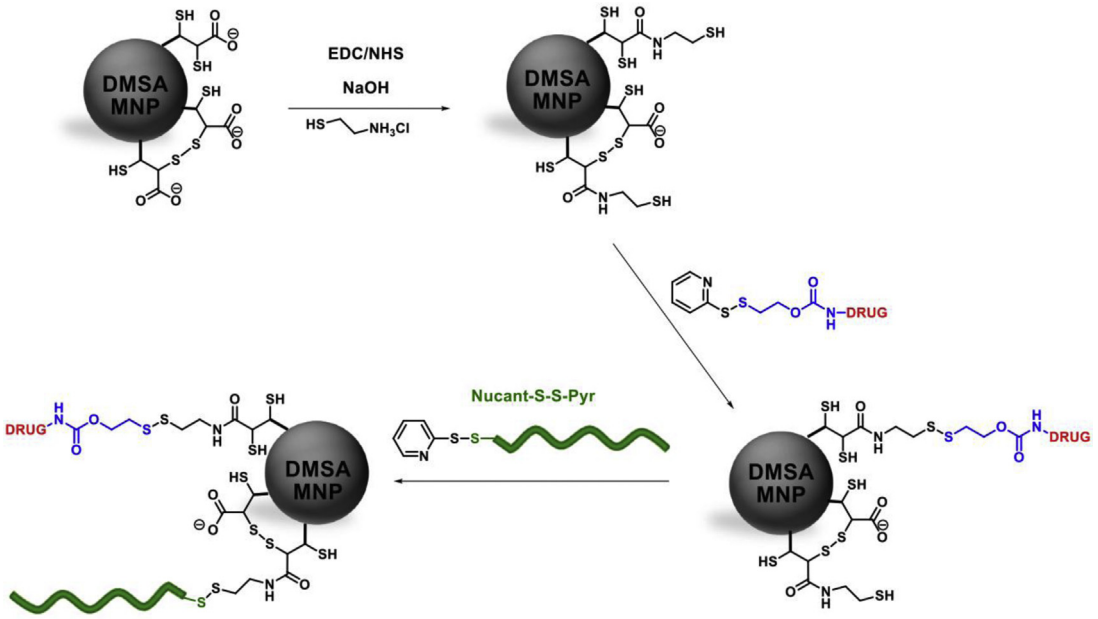

Fig. 2. General scheme of functionalization of DMSA-MNPs.

washed with brine to eliminate electrostatically immobilized Nucant and then with water. From the collected supernatant the covalently immobilized Nucant onto DMSA-MNPs was determined by quantification of the 2-pyridinethione released ($\lambda_{max} = 343$ nm, $\varepsilon_{343\ nm} = 8080$ L mol^{-1} cm^{-1}, Fig. S.3).

The yield of immobilization was 70% (5 μmol N6L/g Fe). The zeta potential of the sample was −41.9 ± 3.3 mV at pH 7.4 with a hydrodynamic diameter of 102.2 ± 0.4 nm.

2.3.2.5. Bi-functionalization of thiolated DMSA-MNPs (MNP-DOX-N6L and MNP-GEM-N6L). 1 mL of aqueous suspension of MNP-DOX at 2.4 mg Fe/mL was mixed with 84 μL of N6L-S-S-Pyr **(5)** solution at 200 μM in water (0.0168 μmol) during 16 h at RT. After reaction, 20 μL of brine were added and the sample was centrifuged 10 min at *5000* × *g* three times to eliminate any electrostatically bound N6L. *UV–Vis* absorption of supernatants was checked to quantify the N6L covalently bound as described in 2.3.2.4. The same protocol was employed for the synthesis of MNP-GEM-N6L.

2.3.3. In vitro drugs release studies

The cumulative drugs release experiments were carried out using two different conditions in order to evaluate the stimuli–response behavior of functionalized DMSA-MNPs toward reducing environment. The release of drugs, from the functionalized DMSA-MNPs was carried out under physiological conditions (pH 7.4 and 37 °C) using two different concentrations of reducing agent (1 μM and 1 mM of 1,4-Dithiothreitol (DTT) to mimic the extracellular and intracellular conditions, respectively). For each experiment, 2.4 mg of functionalized MNPs (or 4.8 mg in the case of the MNP-GEM and MNP-DOX) were dissolved in 1 mL of 10 mM phosphate buffer at pH 7.4 containing 1 μM of DTT, or 10 mM phosphate buffer pH 7.4 containing 1 mM DTT and incubated at 37 °C. The amount of each drug released was determined by different methods at regular time intervals. The percentage of drug released was calculated from a standard calibration curve of free drug solution. The amount of DOX released was analyzed by measuring the absorbance of the sample at 495 nm with *UV–vis* spectrophotometer (Fig. S.5). The amount of released GEM was analyzed by HPLC using a C-18 column, mobile phase water/acetonitrile 80/20, at flow rate of 0.3 mL/min, measuring the absorbance at 270 nm (Fig. S.6). The amount of released N6L was analyzed using Bradford's method [34] by measuring the absorbance of the sample at 595 nm with the UV–Visible spectrophotometer (Fig. S.7).

3. Results and discussion

The use of disulfide bonds for covalent attachment and triggered intracellular delivery of the drugs relies on the following strategy. First, a modification of the drug to introduce pyridyldisulfide group is required to promote the reaction with pre-thiolated DMSA-MNPs. At the same time, the pyridyl group in the activated molecules (Fig. 1) will allow to quantify the covalently linked drug by measuring the pyridine-2-thione released during the coupling reaction with MNPs (Fig. 2). In addition, the presence of disulfide bonds between DMSA-MNPs and drugs will permit the controlled intracellular release of the drug under intracellular reducing conditions. What is more, the linker design allows to release the drug without any chemical modification, since the free thiol generated upon disulfide cleavage is able to attack the carbonate moiety favored by the formation of a five member ring, leaving the drug unaltered (Fig. 3). This kind of autoimmolative-linker has been used previously conjugated with targeting molecules [24], but as far as we know it has not been used to immobilize drugs onto the MNPs surface.

3.1. Synthesis of drugs derivatives

The synthesis of drug derivatives was achieved in three steps. Starting from commercially available aldrithiol, 2-mercaptoethanol was added to give rise to compound **1** by a simple disulfide exchange reaction. Then, the primary alcohol was converted in the electrophilic carbonate compound **2** by the reaction with bis(4-nitrophenyl) carbonate (Fig. 1). Finally, the corresponding chemotherapeutic drugs were incorporated to this linker through the carbonate moiety by the nucleophilic substitution of the 4-

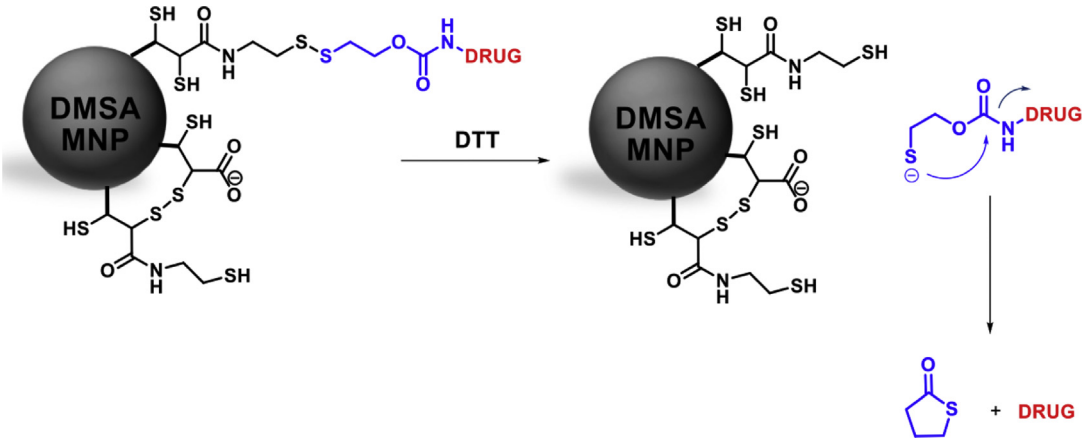

Fig. 3. Scheme of drug release strategy in presence of reducing agent (DTT).

nitrophenol leaving group. Nucant derivative (**5**) was obtained by reaction of cysteine modified Nucant with aldrithiol.

3.2. Functionalization of DMSA-MNPs

3.2.1. Pre-activation of DMSA-MNPs by cysteamine

DMSA coated nanoparticles have thiol groups available from the DMSA. However, we have observed that the amount of these groups on the particles surface decreases over time and at different pHs [35]. Therefore, the DMSA-MNPs employed in this work have been stabilized by basic treatment in order to favor disulfide bonds formation between DMSA molecules of the coating [5]. Then, to assure a fixed and controlled amount of free thiol functions on DMSA-MNPs, an activation step was performed before the functionalization with the desired molecules. The introduction of thiol groups on the surface of DMSA-MNPs was achieved by reaction between cysteamine hydrochloride and carboxylate groups of DMSA-MNPs in presence of EDC/NHS in basic medium (Fig. 2). Particularly, the reaction of 50 μmol of cysteamine/g Fe led to a maximum of 30 μmol of reactive thiol groups/g Fe. The pre-activated DMSA-MNPs are stable at physiological pH. DMSA-MNPs thiolated present a zeta potential of −54.5 ± 2.1 mV and a hydrodynamic diameter of 59.0 ± 1.8 nm whereas DMSA-MNPs present a zeta potential of −60.1 ± 2.1 mV and a hydrodynamic diameter of 53.1 ± 0.9 nm.

3.2.2. Covalent attachment of Doxorubicin and Gemcitabine on pre-activated DMSA-MNPs

The reaction of modified DOX and GEM with pre-activated DMSA-MNPs led to stable colloidal formulations of functionalized DMSA-MNPs with 32 μmol DOX/g Fe and 30 μmol GEM/g Fe, respectively. As discussed previously, a decisive parameter is the colloidal stability in physiological medium. In this case, a slight difference was observed in the zeta potential and the hydrodynamic diameter of these particles compared with DMSA-MNPs. The immobilization yields were 64% for DOX and 60% for GEM with loads of 32 μmol DOX/g Fe and 30 μmol GEM/g Fe, respectively. Zeta potentials and hydrodynamic diameters obtained for each formulation are showed in Table 1.

Table 1
Characterization of mono-functionalized DMSA-MNPs.

Sample	Zeta potential (mV)	Hydrodynamic diameter (nm)
DMSA-MNPs	−60.1 ± 2.1 mV	53.1 ± 0.9 nm
MNP-DOX	−45.4 ± 0.7 mV	86.3 ± 3.1 nm
MNP-GEM	−43.0 ± 1.1 mV	82.6 ± 1.5 nm

3.2.3. Covalent attachment of Nucant pseudopeptide on pre-activated DMSA-MNPs

The functionalization was achieved by the formation of disulfide bonds between the reactive thiols of the modified DMSA-MNPs and the thiol-activated Nucant pseudopeptide. The analysis of the 2-pyridinethione released during the reaction allowed the quantification of the covalently bound N6L (Fig. S.3). The standard load obtained of covalently linked N6L was 5 μmol N6L/g Fe, which is lower than in the cases of DOX and GEM. This difference could be due to the size of Nucant, which is almost 10 times larger than DOX and GEM as well as to the positive charge displayed at physiological pH. Indeed, the addition of high amounts of activated N6L neutralizes all the negative charges of the DMSA coating leading to the aggregation of the MNPs. We have observed that particles with 5 μmol N6L/g Fe are stable at pH 7.4 with a zeta potential of −41.9 ± 3.3 mV and a hydrodynamic diameter of 102.2 ± 0.4 nm.

3.2.4. Bi-functionalization of DMSA-MNPs with drug (DOX or GEM) and N6L (MNP-DOX-N6L and MNP-GEM-N6L)

The last step of this study is the preparation of bi-functionalized DMSA-MNPs in order to provide a targeting moiety, Nucant pseudopeptide, and an anticancer drug, GEM or DOX. The general strategy began with the immobilization of the drug (DOX or GEM) as described previously. Once the drugs have been conjugated there are still enough thiol moieties available in the MNP to introduce the N6L. This order of functionalization is also driven by the fact that the N6L is larger than DOX and GEM and might cause steric hindrance if placed first on the MNPs surface. The conjugation yield of N6L was 70% (5 μmol N6L/g Fe) in particles loaded with DOX or GEM. Zeta potentials and hydrodynamic diameters obtained for each formulation are showed in Table 2.

3.3. In vitro drugs release studies

In this work, we studied the release of drugs in different media and concentrations of reducing agent for the different types of functionalized DMSA-MNPs (mono- and bi-functionalized). As Nucant pseudopeptide acts as both targeting moiety and cytotoxic agent, release studies have been carried out with DMSA-MNPs

Table 2
Characterization of bi-functionalized DMSA-MNPs.

Sample	Zeta potential (mV)	Hydrodynamic diameter (nm)
MNP-DOX-N6L	−38.5 ± 1.4 mV	144.1 ± 0.8 nm
MNP-GEM-N6L	−36.5 ± 4.2 mV	118.1 ± 0.7 nm

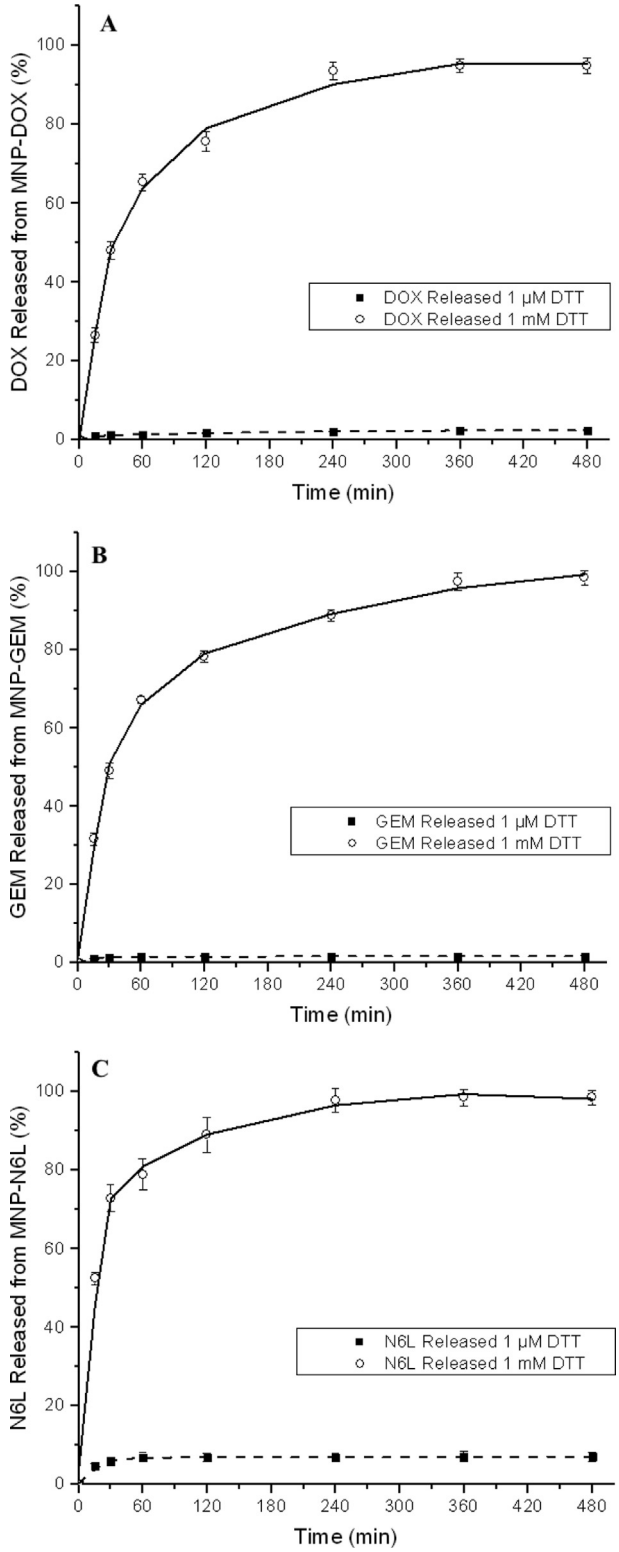

Fig. 4. Release kinetics of mono-functionalized DMSA-MNPs with DOX (A), GEM (B) and N6L (C) (1 μM DTT, filled squares and dashed line and 1 mM DTT, empty circles and solid line).

functionalized with DOX, GEM and N6L, and with bi-functionalized MNPs. Two concentrations of DTT were employed in order to mimic extracellular and intracellular medium, DTT = 1 μM and DTT = 1 mM, respectively.

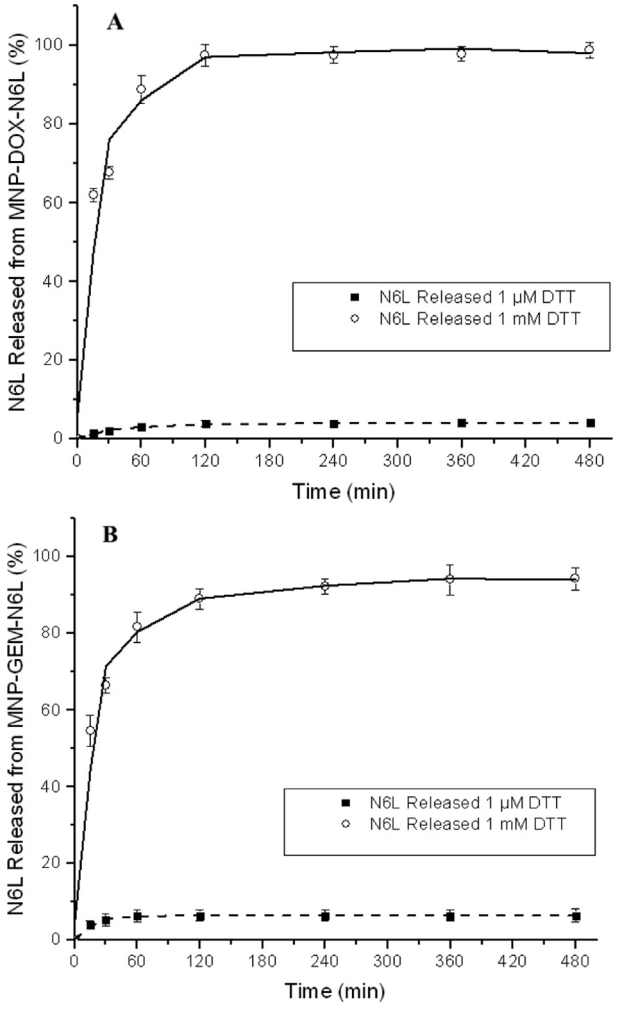

Fig. 5. Release kinetics of N6L pseudopeptide from bi-functionalized DMSA-MNPs. MNP-DOX-N6L (A) and MNP-GEM-N6L (B), (1 μM DTT, filled squares and dashed line and 1 mM DTT, empty circles and solid line).

The release of the attached molecules from the functionalized DMSA-MNPs was monitored during 12 h in PB buffer (10 mM phosphate pH 7.4). *In vitro* drug release experiments were first done with mono-functionalized DMSA-MNPs using intracellular conditions (1 mM of DTT) and extracellular conditions (1 μM of DTT) at 37 °C (Fig. 4).

The three mono-functionalized formulations showed a 95% release when treated with 1 mM DTT after 8 h, although after 1 h almost 70% of cargo was released. On the other hand, when the particles were exposed to extracellular conditions (1 μM DTT), only 7% of the cargo was released after 8 h. In Fig. 5, *in vitro* release experiments of N6L in the both bi-functionalized formulations are shown, using the same experimental conditions.

The release experiments of N6L from bi-functionalized formulations showed the same profiles than the ones observed for the mono-functionalized formulation of Nucant (MNP-N6L).

Finally, release kinetics of DOX and GEM from the two bi-functionalized formulations are presented in Fig. 6. The experimental conditions were the same as in the previous example.

Similar values of release were observed on mono and bi-functionalized formulations when exposed to intracellular conditions, releasing 95% of the drugs after 8 h.

These results show that a reducing environment caused the rapid dissociation of the drugs from MNP and that the release rate

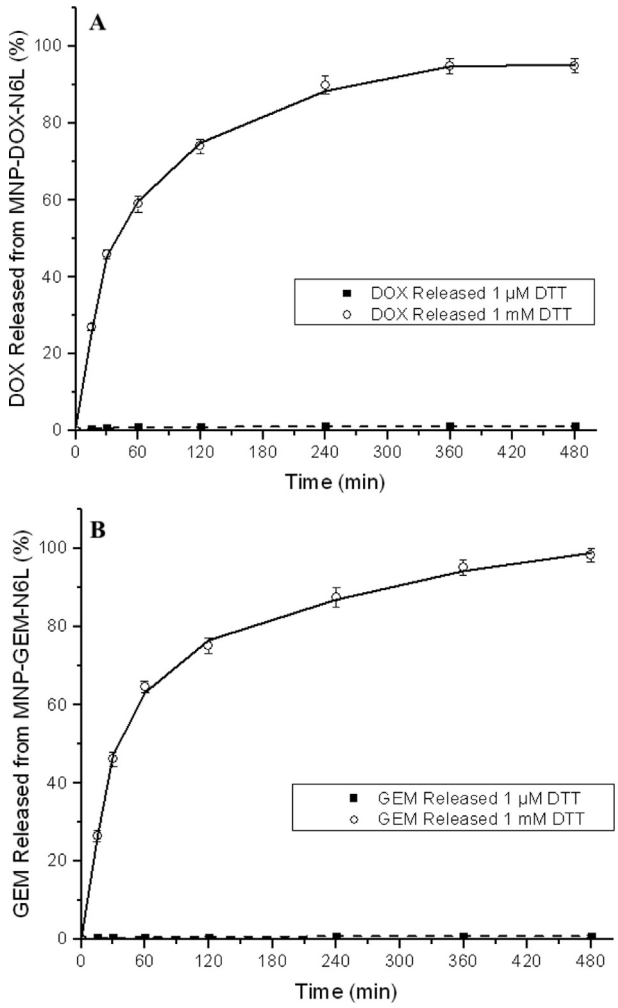

Fig. 6. Release kinetics of DOX from MNP-N6L-DOX (A) and GEM from MNP-N6L-GEM (B) (DTT 1 μM, filled squares and dashed line and DTT 1 mM, empty circles and solid line).

was strongly dependent on the reducing environment. We can also conclude that the bi-functionalization does not affect the release of the drug and the N6L. What is more, the loads of the described nanoparticles are only released under reducing conditions as those present in cytoplasm and lysosomal environments.

4. Conclusions

This study shows optimized strategies for controlled and quantitative functionalization of DMSA coated iron oxide nanoparticles with molecules such as commercially anticancer drugs (Gemcitabine and Doxorubicin) and a targeting and cytotoxic agent (Nucant pseudopeptide). This strategy is modular and generally applicable thus, could be easily implemented for the immobilization of other molecules of interest.

The colloidal stability of every formulation is preserved in physiological conditions, with drug loads of 32 μmol/g Fe and 30 μmol/g Fe for DOX and GEM, respectively. These nanostructures can carry drugs to final concentrations of 16 μM and 15 μM of DOX and GEM, respectively with iron doses of 0.5 mg Fe/mL, commonly used *in vitro* for DMSA-MNPs [36,37]. Therefore, these nanocarriers can deliver drugs at local concentrations much higher than the IC50 values reported for different cell lines (IC50 of DOX in MCF-7 cells is 0.23 μM [38] and IC50 of GEM in Panc-1 cells is 0.11 μM [39]). The developed strategy permits a controlled release of the drugs only under a reducing environment that mimics the intracellular media. Additionally, it is shown the bi-functionalization of DMSA-MNPs with drugs and a peptide that is both a targeting and anticancer agent. These multifunctional nanostructures still exhibit controlled release properties of the two ligands.

The developed nanostructures described here have great potential in directed controlled drug release strategies in nanomedicine, and promise to overcome already present drug resistance problems in cancer treatment. *In vitro* and *in vivo* experiments are being carried out in order to explore the applicability of the functionalized MNP presented in this work.

Acknowledgments

This work was supported by EU-FP7 MULTIFUN project (n° 262943). The authors thank Dr. Gorka Salas, Leonor de La Cueva and Rebeca Amaro for providing DMSA-MNPs, and Prof. José Courty for providing the Nucant pseudopeptide.

Appendix A. Supplementary data

Supplementary data related to this article can be found at http://dx.doi.org/10.1016/j.ejmech.2014.05.078.

References

[1] S.M. Moghimi, A.C. Hunter, J.C. Murray, Nanomedicine: current status and future prospects, FASEB J. 19 (2005) 311–330.
[2] A.K. Gupta, M. Gupta, Synthesis and surface engineering of iron oxide nanoparticles for biomedical applications, Biomaterials 26 (2005) 3995–4021.
[3] O. Veiseh, J.W. Gunn, M. Zhang, Design and fabrication of magnetic nanoparticles for targeted drug delivery and imaging, Adv. Drug Deliv. Rev. 62 (2010) 284–304.
[4] J.D. Byrne, T. Betancourt, L. Brannon-Peppas, Active targeting schemes for nanoparticle systems in cancer therapeutics, Adv. Drug Deliv. Rev. 60 (2008) 1615–1626.
[5] B. Book Newell, Y. Wang, J. Irudayaraj, Multifunctional gold nanorod theragnostics probed by multi-photon imaging, Eur. J. Med. Chem. 48 (2012) 330–337.
[6] G. Salas, C. Casado, F.J. Teran, R. Miranda, C.J. Serna, M.D.P. Morales, Controlled synthesis of uniform magnetite nanocrystals with high-quality properties for biomedical applications, J. Mater. Chem. 22 (2012) 21065.
[7] M. Marciello, V. Connord, S. Veintemillas-Verdaguer, M.A. Vergés, J. Carrey, M. Respaud, et al., Large scale production of biocompatible magnetite nanocrystals with high saturation magnetization values through green aqueous synthesis, J. Mater. Chem. B 1 (2013) 5995–6004.
[8] F. Meyer-Losic, J. Quinonero, V. Dubois, B. Alluis, M. Dechambre, M. Michel, et al., Improved therapeutic efficacy of doxorubicin through conjugation with a novel peptide drug delivery technology (Vectocell), J. Med. Chem. 49 (2006) 6908–6916.
[9] H. Burris, M. Moore, J. Andersen, M.R. Green, M.L. Rothenberg, M.R. Modiano, et al., Improvements in survival and clinical benefit with gemcitabine as first-line therapy for patients with advanced pancreas cancer: a randomized trial, J. Clin. Oncol. 15 (1997) 2403–2413.
[10] W. Plunkett, P. Huang, V. Gandhi, Preclinical characteristics of gemcitabine, Anticancer Drugs 6 (1995) 7–13.
[11] L.W. Hertel, G.B. Boder, J.S. Kroin, S.M. Rinzel, G.A. Poore, G.C. Todd, G.B. Grindey, Evaluation of the antitumor activity of gemcitabine (2′,2′-difluoro-2′-deoxycytidine), Cancer Res. 50 (1990) 4417–4422.
[12] C.F. Thorn, C. Oshiro, S. Marsh, T. Hernandez-Boussard, H. McLeod, T.E. Klein, R.B. Altman, Doxorubicin pathways: pharmacodynamics and adverse effects, Pharmacogenet. Genomics 21 (2011) 440–446.
[13] L. Harivardhan Reddy, Catherine Dubernet, Sinda Lepetre Mouelhi, Pierre Emmanuel Marque, Didier Desmaele, Patrick Couvreur, A new nanomedicine of gemcitabine displays enhanced anticancer activity in sensitive and resistant leukemia types, J. Control Release 124 (1–2) (4 December 2007) 20–27.
[14] X. Zeng, R. Morgenstern, A.M. Nyström, Nanoparticle-directed sub-cellular localization of doxorubicin and the sensitization breast cancer cells by circumventing GST-mediated drug resistance, Biomaterials 35 (2014) 1227–1239.
[15] L.S. Jabr-Milane, L.E. van Vlerken, S. Yadav, M.M. Amiji, Multi-functional nanocarriers to overcome tumor drug resistance, Cancer Treat. Rev. 34 (2008) 592–602.
[16] D. Destouches, N. Page, Y. Hamma-Kourbali, V. Machi, O. Chaloin, S. Frechault, C. Birmpas, P. Katsoris, J. Beyrath, P. Albanese, M. Maurer, G. Carpentier, J.-

M. Strub, A. Van Dorsselaer, S. Muller, D. Bagnard, J.P. Briand, J. Courty, A simple approach to cancer therapy afforded by multivalent pseudopeptides that target cell-surface nucleoproteins, Cancer Res. 71 (2011) 3296–3305.
[17] D. Destouches, E. Huet, M. Sader, S. Frechault, G. Carpentier, F. Ayoul, J.-P. Briand, S. Menashi, J. Courty, Multivalent pseudopeptides targeting cell surface nucleoproteins inhibit cancer cell invasion through tissue inhibitor of metalloproteinases 3 (TIMP-3) release, J. Biol. Chem. 287 (2012) 43685–43693.
[18] D. Destouches, D. El Khoury, Y. Hamma-Kourbali, B. Krust, P. Albanese, P. Katsoris, G. Guichard, J.P. Briand, J. Courty, A.G. Hovanessian, Suppression of tumor growth and angiogenesis by a specific antagonist of the cell-surface expressed nucleolin, PLoS One 3 (2008) e2518.
[19] R. Mejías, S. Pérez-Yagüe, L. Gutiérrez, L.I. Cabrera, R. Spada, P. Acedo, C.J. Serna, F.J. Lázaro, A. Villanueva, M.D.P. Morales, D.F. Barber, Dimercaptosuccinic acid-coated magnetite nanoparticles for magnetically guided in vivo delivery of interferon gamma for cancer immunotherapy, Biomaterials 32 (2011) 2938–2952.
[20] A.Z. Mirza, H. Shamshad, Preparation and characterization of doxorubicin functionalized gold nanoparticles, Eur. J. Med. Chem. 46 (2011) 1857–1860.
[21] S.S. Banerjee, D.-H. Chen, Multifunctional pH-sensitive magnetic nanoparticles for simultaneous imaging, sensing and targeted intracellular anticancer drug delivery, Nanotechnology 19 (2008) 505104.
[22] C. Fang, F.M. Kievit, O. Veiseh, Z.R. Stephen, T. Wang, D. Lee, R.G. Ellenbogen, M. Zhang, Fabrication of magnetic nanoparticles with controllable drug loading and release through a simple assembly approach, J. Control Release 162 (2012) 233–241.
[23] H. Wang, T.B. Shrestha, M.T. Basel, R.K. Dani, G.-M. Seo, S. Balivada, M.M. Pyle, H. Prock, O.B. Koper, P.S. Thapa, D. Moore, P. Li, V. Chikan, D.L. Troyer, S.H. Bossmann, Magnetic-Fe/Fe(3)O(4)-nanoparticle-bound SN38 as carboxylesterase-cleavable prodrug for the delivery to tumors within monocytes/macrophages, Beilstein J. Nanotechnol. 3 (2012) 444–455.
[24] F. Cengelli, J.A. Grzyb, A. Montoro, H. Hofmann, S. Hanessian, L. Juillerat-Jeanneret, Surface-functionalized ultrasmall superparamagnetic nanoparticles as magnetic delivery vectors for camptothecin, ChemMedChem 4 (2009) 988–997.
[25] G.Y. Lee, W.P. Qian, L. Wang, Y.A. Wang, C.A. Staley, M. Satpathy, S. Nie, H. Mao, L. Yang, Theranostic nanoparticles with controlled release of gemcitabine for targeted therapy and MRI of pancreatic cancer, ACS Nano 7 (2013) 2078–2089.
[26] M. Chiper, K. Hervé Aubert, A. Augé, J.-F. Fouquenet, M. Soucé, I. Chourpa, Colloidal stability and thermo-responsive properties of iron oxide nanoparticles coated with polymers: advantages of Pluronic® F68-PEG mixture, Nanotechnology 24 (2013) 395605.
[27] C. Dionigi, Y. Piñeiro, A. Riminucci, M. Bañobre, Regulating the thermal response of PNIPAM hydrogels by controlling the adsorption of magnetite nanoparticles, Appl. Phys. A 114 (2014) 585–590.
[28] G. Saito, J. Swanson, K. Lee, Drug delivery strategy utilizing conjugation via reversible disulfide linkages: role and site of cellular reducing activities, Adv. Drug Deliv. Rev. 55 (2003) 199–215.
[29] A. Meister, M.E. Anderson, Glutathione, Annu. Rev. Biochem. 52 (1983) 711–760.
[30] W.G. Kirlin, J. Cai, S.A. Thompson, D. Diaz, T.J. Kavanagh, D.P. Jones, Glutathione redox potential in response to differentiation and enzyme inducers, Free Radic. Biol. Med. 27 (1999) 1208–1218.
[31] S.L. Blair, P. Heerdt, S. Sachar, A. Abolhoda, S. Hochwald, H. Cheng, M. Burt, Glutathione metabolism in patients with non-small cell lung cancers, Cancer Res. 57 (1997) 152–155.
[32] M. Lapeyre, J. Leprince, M. Massonneau, H. Oulyadi, P.-Y. Renard, A. Romieu, G. Turcatti, H. Vaudry, Aryldithioethyloxycarbonyl (Ardec): a new family of amine protecting groups removable under mild reducing conditions and their applications to peptide synthesis, Chemistry 12 (2006) 3655–3671.
[33] A. Satyam, Design and synthesis of releasable folate-drug conjugates using a novel heterobifunctional disulfide-containing linker, Bioorg. Med. Chem. Lett. 18 (2008) 3196–3199.
[34] M.M. Bradford, A rapid and sensitive method for the quantitation of microgram quantities of protein utilizing the principle of protein-dye binding, Anal. Biochem. 72 (1976) 248–254.
[35] N. Fauconnier, J. Pons, J. Roger, A. Bee, Thiolation of maghemite nanoparticles by dimercaptosuccinic acid, J. Colloid Interface Sci. 194 (1997) 427–433.
[36] M. Calero, L. Gutiérrrez, G. Salas, Y. Luengo, A. Lázaro, P. Acedo, M.P. Morales, R. Miranda, A. Villanueva, Efficient and safe internalization of magnetic iron oxide nanoparticles: two fundamental requirements for biomedical applications, Nanomedicine (2013) 1–11.
[37] R. Mejías, L. Gutiérrez, G. Salas, S. Pérez-Yagüe, T.M. Zotes, F.J. Lázaro, M.P. Morales, D.F. Barber, Long term biotransformation and toxicity of dimercaptosuccinic acid-coated magnetic nanoparticles support their use in biomedical applications, J. Control Release 171 (2013) 225–233.
[38] A.-M.M. Osman, H.M. Bayoumi, S.E. Al-Harthi, Z.A. Damanhouri, M.F. Elshal, Modulation of doxorubicin cytotoxicity by resveratrol in a human breast cancer cell line, Cancer Cell Int. 12 (2012) 47.
[39] C. Ramachandran, A. Resek, Potentiation of gemcitabine by Turmeric Force™ in pancreatic cancer cell lines, Oncol. Rep. 23 (2010) 1529–1535.